Frontiers of Information Technology & Electronic Engineering
www.zju.edu.cn/jzus; engineering.cae.cn; www.springerlink.com
ISSN 2095-9184 (print); ISSN 2095-9230 (online)
E-mail: jzus@zju.edu.cn

# Deformable image registration with geometric changes

Yu LIU, Bo ZHU[†‡]

(*School of Aeronautics and Astronautics, Zhejiang University, Hangzhou 310027, China*)

[†]E-mail: zhubomm@gmail.com

Received Feb. 5, 2015; Revision accepted June 1, 2015; Crosschecked Sept. 9, 2015

**Abstract:** Geometric changes present a number of difficulties in deformable image registration. In this paper, we propose a global deformation framework to model geometric changes whilst promoting a smooth transformation between source and target images. To achieve this, we have developed an innovative model which significantly reduces the side effects of geometric changes in image registration, and thus improves the registration accuracy. Our key contribution is the introduction of a sparsity-inducing norm, which is typically L1 norm regularization targeting regions where geometric changes occur. This preserves the smoothness of global transformation by eliminating local transformation under different conditions. Numerical solutions are discussed and analyzed to guarantee the stability and fast convergence of our algorithm. To demonstrate the effectiveness and utility of this method, we evaluate it on both synthetic data and real data from traumatic brain injury (TBI). We show that the transformation estimated from our model is able to reconstruct the target image with lower instances of error than a standard elastic registration model.

**Key words:** Geometric changes, Image registration, Sparsity, Traumatic brain injury (TBI)
**doi:**10.1631/FITEE.1500045 **Document code:** A **CLC number:** TP391.4

## 1 Introduction

Deformable image registration has been used as a vital tool in a wide range of fields in image analysis, for example, atlas building, object tracking, and automatic target recognition. It can also be used in disease diagnosis and treatment verification by comparing patients' data with an anatomical atlas for clinical studies. Standard image registration methods predominantly measure structural similarity between a source and a target image. The standard method of defining similarity is based on intensity discrepancy, cross correlation (CC), or mutual information. The earliest attempt to measure high dimensional non-rigid transformation in a medical image system was proposed by Bajcsy and Broit (1982) after image matching rules were described in a hierarchical searching technique (Hall, 1979). Herbin *et al*. (1989) proposed a mathematical model to further study registration for dissimilar images by estimating the unknown transformation as a parameter. These methods, as discussed above, solve the registration problem in a small deformation framework. Work has also been done to optimize registration over a large deformation field. Christensen *et al*. (1996) presented a fluid dynamic system which allows large magnitude deformations by numerically solving partial differential equations associated with a constrained problem. Subsequently, to reduce the computation complexity of processing data with high dimensionality in Christensen *et al*. (1996), Beg *et al*. (2005) introduced the concept of tracking optimal flow (the shortest transforming path under a regularized metric) between template and target images. They defined a large deformation diffeomorphic metric mapping and explained the geodesic deformation flowing along the time-dependent velocity fields.

Statistical modeling is commonly used in the image registration area. Markov chain Monte Carlo sampling coupled with the Markov random field has

[‡] Corresponding author
ORCID: Bo ZHU, http://orcid.org/0000-0002-9801-2223

been proved to be a powerful tool for both parametric and non-parametric registration problems (Luck *et al*., 2000; Richard and Samson, 2007; Zhang *et al*., 2013). This algorithm samples a new displacement vector which is assumed to have joint Gaussian distribution at exactly one state in each iteration. A state space model (Trouvé and Younes, 2005) was effectively established by constructing the energy functional using the summation of similarity and regularization terms. Simulated annealing was applied to drive the total energy down until converging to a global minimum.

However, the large geometric and intensity changes, combined with limited image information available, make image registration challenging under these settings. Direct application of current methodology may lead to an unpredictable and unrealistic estimation of the deformation field. For instance, the infiltration caused by traumatic injury, tumor, or blood perfusion dramatically decreases the traditional registration's accuracy due to the topological changes and missing local information. It distorts the model's progress towards a global optimal transformation. This is further compounded by slow convergence and poor numerical stability. To solve this problem, Niethammer *et al*. (2011) developed a geometric metamorphosis formulation that takes geometric changes into consideration by registering those areas separately from the global image registration problem. To the best of our knowledge, our model proposed in this paper is the first to estimate an optimal global transformation whilst seeking control of the side effects of geometric changes in the same framework. To achieve this, we have designed a sparse model which provides different levels of constraints on local deformations, and which uses a new energy optimization scheme derived from the inverse consistent principle (Christensen and Johnson, 2001) to preserve the topology and uniquely describe the correspondence between images. A numerical dual algorithm is used to speed up the convergence. We demonstrate the utility of our approach on both synthetic data and real traumatic brain injury (TBI) data from patients. Experimental results show that our method outperforms traditional elastic image registration by significantly improving the registration accuracy.

## 2 Background

The main idea behind our model is enforcing a sparsity to eliminate the side effects of the geometric change area. Before introducing our model, we review the current framework of image registration.

Our model is based on inverse consistency image registration as proposed in Christensen *et al*. (1996). It is stated as finding the optimal transformation $p$ that maps the template image $\boldsymbol{I}_0$ into the target image $\boldsymbol{I}_1$, where $\boldsymbol{x}$ is a column vector which denotes each voxel coordinate of an image. In this framework $\boldsymbol{I}_0$, $\boldsymbol{I}_1 \in L^2(\Omega, \mathbb{R})$, where $\Omega$ denotes the discretized grid on the continuous image domain. $L^2(\Omega, \mathbb{R})$ is the infinite dimensional Hilbert space. One of the classical measurements to determine an optimal transformation $p(\boldsymbol{x})$ is based on image intensity discrepancy and smoothness penalty on the image transformation. The common cost function is given by

$$\min E_p = \int_\Omega \left( \frac{1}{2} \left\| \boldsymbol{I}_1(\boldsymbol{x}) - \boldsymbol{I}_0(\boldsymbol{x} + p(\boldsymbol{x})) \right\|^2 + \lambda \left| \nabla p(\boldsymbol{x}) \right| \right), \tag{1}$$

where $\lambda$ is a balance parameter between the image match term and regularization. The term $\lambda|\nabla p(\boldsymbol{x})|$ is the total variation regularization that smooths the deformation field $p$ but still preserves the edge information of the deformation field.

A typical problem with image matching registration in Eq. (1) is that minimizing the similarity function does not uniquely determine the correspondence between two images. In addition, the similarity based cost function has a large number of local minima, due to the complexity of the images and the high dimensionality of the transformation. This causes difficulties in producing a consistent set of transformations. To overcome the correspondence ambiguities, Christensen and Johnson (2001) derived a joint estimation of forward transformation from image $\boldsymbol{I}_0$ to $\boldsymbol{I}_1$ and its inverse (backward) transformation from $\boldsymbol{I}_1$ to $\boldsymbol{I}_0$ simultaneously. One advantage of this model is that it can encourage a consistent transformation between images by including additional correspondence information from backward registration. Another advantage is that the difference

between a deformed template and a deformed target is smaller than that between a deformed template and a fixed target, or that between a deformed target and a fixed template. Thus, the deformation error in the former case is smaller, which results in a more accurate and smoother registration result. The energy formulation of inverse consistency is defined by

$$\begin{aligned}&\min E_{p,q}=\\&\int_{\Omega}\Big(\frac{1}{2}\|\boldsymbol{I}_1(\boldsymbol{x})-\boldsymbol{I}_0(\boldsymbol{x}+p(\boldsymbol{x}))\|^2+\lambda|\nabla p(\boldsymbol{x})|\\&+\frac{\beta}{2}\|p(\boldsymbol{x})+q(\boldsymbol{x}+p(\boldsymbol{x}))\|^2\\&+\frac{1}{2}\|\boldsymbol{I}_1(\boldsymbol{x}+q(\boldsymbol{x}))-\boldsymbol{I}_0(\boldsymbol{x})\|^2+\gamma|\nabla q(\boldsymbol{x})|\\&+\frac{\eta}{2}\|q(\boldsymbol{x})+p(\boldsymbol{x}+q(\boldsymbol{x}))\|^2\Big),\end{aligned}\tag{2}$$

where $p$ denotes the forward transformation, and $q$ is the backward transformation. $\lambda$ and $\gamma$ are the balance parameters for forward and backward transformations, respectively. Assume that $p$ and $q$ are continuous differentiable transformations that map onto each other and have positive Jacobian for all $\boldsymbol{x}\in\Omega(p\cup q)$. This implies local one-to-one mapping for both directional transformations, and therefore has a local inverse. Based on the above assumption, it is theoretically possible to iteratively find a point in $q$ so that $p(\boldsymbol{x})+q(\boldsymbol{x}+p(\boldsymbol{x}))=0$ or a point in $p$ so that $q(\boldsymbol{x})+p(\boldsymbol{x}+q(\boldsymbol{x}))=0$. However, in practice, it is more reasonable to express this as $p(\boldsymbol{x})+q(\boldsymbol{x}+p(\boldsymbol{x}))\cong 0$ for all $q(\boldsymbol{x})$ and $q(\boldsymbol{x})+p(\boldsymbol{x}+q(\boldsymbol{x}))\cong 0$ for all $p(\boldsymbol{x})$. $\beta$, $\eta\in[0, 1]$ are parameters which determine the strength of inverse consistency: the larger $\beta$ and $\eta$ are, the more inverse consistency is enforced.

## 3 The proposed algorithm

As noted in the introduction, although geometric changes might be appropriate for traditional registration models with low dimensional image transformation, a direct application of classical deformable registration methods produces inaccurate information in estimating deformation fields. To solve this problem, Trouvé and Younes (2005) proposed an image metamorphosis method which uses weak models to transform the image from the template to the target image smoothly; however, the transformations or composition of the pathologies estimated in this method do not have an explicit formulation. We will propose an innovative approach which is related to the classical registration model but identifies geometric change areas that cannot be matched due to a missing correspondence (non-invertible). The pathological deformations are then detected using underlying image deformations. The energy functionality of our model is defined as

$$\begin{aligned}&\min E_{p,q,b,c}=\\&\int_{\Omega}\Big(\frac{1}{2}\|\boldsymbol{I}_1(\boldsymbol{x})-\boldsymbol{I}_0(\boldsymbol{x}+p(\boldsymbol{x}))\|^2+\lambda|\nabla p(\boldsymbol{x})|\\&+\frac{\beta}{2}\|p(\boldsymbol{x})+q(\boldsymbol{x}+p(\boldsymbol{x}))+b(\boldsymbol{x})\|^2+\varepsilon|b(\boldsymbol{x})|\\&+\frac{1}{2}\|\boldsymbol{I}_1(\boldsymbol{x}+q(\boldsymbol{x}))-\boldsymbol{I}_0(\boldsymbol{x})\|^2+\gamma|\nabla q(\boldsymbol{x})|\\&+\frac{\eta}{2}\|q(\boldsymbol{x})+p(\boldsymbol{x}+q(\boldsymbol{x}))+c(\boldsymbol{x})\|^2+\theta|c(\boldsymbol{x})|\Big),\end{aligned}\tag{3}$$

where $b$ and $c$ are used to identify the non-invertible area. Ideally, if the forward transformation $p(\boldsymbol{x})$ and backward transformation $q(\boldsymbol{x}+p(\boldsymbol{x}))$ are continuously invertible, values in $b$ and $c$ become zero; otherwise, non-zero values are produced. The sparsity term forces the invertible area to be registered as exactly zero, but keeps the non-invertible area regularized. In other words, $|b(\boldsymbol{x})|>0$ denotes a non-invertible area and $|b(\boldsymbol{x})|=0$ denotes an invertible area. $\varepsilon$ and $\theta$ are fudge factors that control the sparsity on the local deformation field.

As all the unknown variables in Eq. (3) are coupled with each other in the energy functional, it is difficult to produce explicit derivatives. To effectively minimize the energy functional on symmetric forward and backward transformations, we use a split variation scheme to rewrite the energy functional with regard to $p$ and $q$ separately:

$$\begin{aligned}&\min E_{p,b}\\&=\int_{\Omega}\Big(\frac{1}{2}\|\boldsymbol{I}_1(\boldsymbol{x})-\boldsymbol{I}_0(\boldsymbol{x}+p(\boldsymbol{x}))\|^2+\lambda|\nabla p(\boldsymbol{x})|\\&+\frac{\beta}{2}\|p(\boldsymbol{x})+q(\boldsymbol{x}+p(\boldsymbol{x}))+b(\boldsymbol{x})\|^2+\varepsilon|b(\boldsymbol{x})|\Big),\end{aligned}\tag{4}$$

$$\min E_{q,c} = \int_{\Omega}\left(\frac{1}{2}\left\|\boldsymbol{I}_1(\boldsymbol{x}+q(\boldsymbol{x}))-\boldsymbol{I}_0(\boldsymbol{x})\right\|^2+\gamma\left|\nabla q(\boldsymbol{x})\right|+\frac{\eta}{2}\left\|q(\boldsymbol{x})+p(\boldsymbol{x}+q(\boldsymbol{x}))+c(\boldsymbol{x})\right\|^2+\theta\left|c(\boldsymbol{x})\right|\right). \tag{5}$$

For the purpose of effective optimization, we will develop an alternative scheme to update the transformations iteratively using the Lucas-Kanade algorithm (Lucas and Kanade, 1981). We use it to estimate additive transformation $\Delta p$ and $\Delta q$ at each iteration rather than updating the transformations $p$ and $q$ directly as in traditional image registration models. This leads to the following optimization formulations of our model:

$$\begin{aligned}\min E_{p,b} &= \int_{\Omega}\left(\frac{1}{2}\left\|\boldsymbol{I}_1(\boldsymbol{x})-\boldsymbol{I}_0(\boldsymbol{x}+p(\boldsymbol{x})+\Delta p(\boldsymbol{x}))\right\|^2\right.\\ &+\lambda\left|\nabla(p(\boldsymbol{x})+\Delta p(\boldsymbol{x}))\right|+\frac{\beta}{2}\|\,p(\boldsymbol{x})+\Delta p(\boldsymbol{x})\\ &\left.+q(\boldsymbol{x}+p(\boldsymbol{x})+\Delta p(\boldsymbol{x}))+b(\boldsymbol{x})\,\|^2+\varepsilon\left|b(\boldsymbol{x})\right|\right),\end{aligned} \tag{6}$$

$$\begin{aligned}\min E_{q,c} &= \int_{\Omega}\left(\frac{1}{2}\left\|\boldsymbol{I}_1(\boldsymbol{x}+q(\boldsymbol{x})+\Delta q(\boldsymbol{x}))-\boldsymbol{I}_0(\boldsymbol{x})\right\|^2\right.\\ &+\gamma\left|\nabla(q(\boldsymbol{x})+\Delta q(\boldsymbol{x}))\right|+\frac{\eta}{2}\|\,q(\boldsymbol{x})+\Delta q(\boldsymbol{x})\\ &\left.+p(\boldsymbol{x}+q(\boldsymbol{x})+\Delta q(\boldsymbol{x}))+c(\boldsymbol{x})\,\|^2+\theta\left|c(\boldsymbol{x})\right|\right),\end{aligned} \tag{7}$$

followed by updating $p(\boldsymbol{x})$ and $q(\boldsymbol{x})$ until they converge, where $p(\boldsymbol{x})\leftarrow p(\boldsymbol{x})+\Delta p(\boldsymbol{x})$ and $q(\boldsymbol{x})\leftarrow q(\boldsymbol{x})+\Delta q(\boldsymbol{x})$.

### 3.1 Numerical solution on data fidelity, regularization, and inverse consistency

Since the problems of forward and backward transformations are symmetrical, we present only algorithms related to forward transformation in this subsection. The solution for backward transformation is the same in reverse.

To reduce computation complexity while gaining more accuracy, we introduce an auxiliary variable $u$, and then minimize the following convex approximation of Eq. (4):

$$\begin{aligned}E_{p,\mu} = &\int\left(\frac{1}{2}\left\|\boldsymbol{I}_1(\boldsymbol{x})-\boldsymbol{I}_0(\boldsymbol{x}+p(\boldsymbol{x})+\Delta p(\boldsymbol{x}))\right\|^2+\lambda\left|\nabla u(\boldsymbol{x})\right|\right.\\ &+\frac{\beta}{2}\left\|p(\boldsymbol{x})+\Delta p(\boldsymbol{x})+q(\boldsymbol{x}+p(\boldsymbol{x})+\Delta p(\boldsymbol{x}))+b(\boldsymbol{x})\right\|^2\\ &\left.+\frac{\mu}{2}\left\|p(\boldsymbol{x})+\Delta p(\boldsymbol{x})-u(\boldsymbol{x})\right\|^2+\varepsilon\left|b(\boldsymbol{x})\right|\right),\end{aligned}$$

where $\mu$ is a small constant such that $u(\boldsymbol{x})$ is a close approximation of $p(\boldsymbol{x})+\Delta p(\boldsymbol{x})$. This convex minimization problem can be optimized by alternating steps between updating $u$ and $\Delta p$ iteratively.

Fixing $\Delta p$, we solve

$$\min_u \int_{\Omega}\left(\lambda\left|\nabla u(\boldsymbol{x})\right|+\frac{\mu}{2}\left\|p(\boldsymbol{x})+\Delta p(\boldsymbol{x})-u(\boldsymbol{x})\right\|^2\right).$$

This function is similar to an image denoising model with total variation regularization as presented by Rudin *et al.* (1992). We apply Chambolle's dual algorithm (Chambolle, 2004) in the optimization procedure as the total variation is a non-differentiable convex function. Our numerical scheme enhances the computational efficiency and accelerates the speed of convergence. We formulate the problem in a fixed point iteration by simply performing a projected gradient descent method. Note that for notational simplicity, we denote $p(\boldsymbol{x})$, $q(\boldsymbol{x})$, $u(\boldsymbol{x})$, $k(\boldsymbol{x})$ on the whole image domain $\Omega$ as $p$, $q$, $u$, $k$, respectively. The closed-form solution for updating $u$ is

$$u = p+\Delta p-\rho\,\mathrm{div}\,k, \tag{8}$$

where $\rho=\lambda/\mu$. We evaluate Eq. (8) by an iterative approximation in the following step:

$$k^{n+1}=\frac{k^n+\tau\nabla(\mathrm{div}\,k^n-(p+\Delta p)/\rho)}{1+\tau\,|\,\nabla(\mathrm{div}\,k^n-(p+\Delta p)/\rho)\,|}$$

with an initial value $k^0=0$ and $\tau$ is the step size.

Fixing $\mu$, we solve

$$\begin{aligned}\min_{\Delta p}\int&\left(\frac{1}{2}\left\|\boldsymbol{I}_1-\boldsymbol{I}_0(\boldsymbol{x}+p(\boldsymbol{x})+\Delta p(\boldsymbol{x}))\right\|^2\right.\\ &+\frac{\beta}{2}\left\|p(\boldsymbol{x})+\Delta p(\boldsymbol{x})+q(\boldsymbol{x}+p(\boldsymbol{x})+\Delta p(\boldsymbol{x}))+b(\boldsymbol{x})\right\|^2\\ &\left.+\frac{\mu}{2}\left\|p(\boldsymbol{x})+\Delta p(\boldsymbol{x})-u(\boldsymbol{x})\right\|^2\right).\end{aligned}$$

Note that the sub-problem above does not depend on the spatial derivatives of $u$, and thus we can solve it using a point-wise method. To obtain the closed-form solution, we use the Taylor expansion to obtain

$$\begin{aligned}&\min_{\Delta p}\int\left(\frac{1}{2}\|\boldsymbol{I}_1-\boldsymbol{I}_0(\boldsymbol{x}+p(\boldsymbol{x})+\Delta p(\boldsymbol{x}))\|^2\right.\\&+\frac{\beta}{2}\|p(\boldsymbol{x})+\Delta p(\boldsymbol{x})+q(\boldsymbol{x}+p(\boldsymbol{x})+\Delta p(\boldsymbol{x}))+b(\boldsymbol{x})\|^2\\&\left.+\frac{\mu}{2}\|p(\boldsymbol{x})+\Delta p(\boldsymbol{x})-u(\boldsymbol{x})\|^2\right).\end{aligned}\tag{9}$$

The optimization problem becomes

$$\begin{aligned}&\min_{\Delta p}\int_{\Omega}\left(\frac{1}{2}\|\boldsymbol{I}_1-\boldsymbol{I}_0(\boldsymbol{x}+p(\boldsymbol{x}))\right.\\&-\Delta p(\boldsymbol{x})\nabla\boldsymbol{I}_0(\boldsymbol{x}+p(\boldsymbol{x}))\|^2\\&+\frac{\beta}{2}\|p(\boldsymbol{x})+\Delta p(\boldsymbol{x})+q(\boldsymbol{x}+p(\boldsymbol{x}))\\&+\Delta p(\boldsymbol{x})\nabla q(\boldsymbol{x}+p(\boldsymbol{x}))+b(\boldsymbol{x})\|^2\\&\left.+\frac{\mu}{2}\|p(\boldsymbol{x})+\Delta p(\boldsymbol{x})-u(\boldsymbol{x})\|^2\right),\end{aligned}\tag{10}$$

where $\Delta p(\boldsymbol{x})^{n+1}=M(\boldsymbol{x})/N(\boldsymbol{x})$. By setting $\frac{\partial}{\partial\Delta p}=0$, we obtain

$$\begin{cases}M(\boldsymbol{x})=\mu(u(\boldsymbol{x})-p(\boldsymbol{x})^n)\\\quad+\nabla\boldsymbol{I}_0(\boldsymbol{x}+p(\boldsymbol{x})^n)(\boldsymbol{I}_1(\boldsymbol{x})-\boldsymbol{I}_0(\boldsymbol{x}+p(\boldsymbol{x})^n))\\\quad-\beta(p(\boldsymbol{x})^n+q^n(\boldsymbol{x}+p(\boldsymbol{x})^n\\\quad+b(\boldsymbol{x})^n))(\boldsymbol{I}+\nabla q^n(\boldsymbol{x}+p(\boldsymbol{x})^n)),\\N(\boldsymbol{x})=\nabla\boldsymbol{I}_0(\boldsymbol{x}+p(\boldsymbol{x})^n)\nabla\boldsymbol{I}_0(\boldsymbol{x}+p(\boldsymbol{x})^n)^{\mathrm{T}}\\\quad+\beta(\boldsymbol{I}+\nabla q^n(\boldsymbol{x}+p(\boldsymbol{x})^n))\\\quad\cdot(\boldsymbol{I}+\nabla q^n(\boldsymbol{x}+p(\boldsymbol{x})^n))^{\mathrm{T}}+\mu\boldsymbol{I}(\boldsymbol{x}),\end{cases}\tag{11}$$

where $\boldsymbol{I}$ is an identity matrix, $\nabla q^n(\boldsymbol{x}+p(\boldsymbol{x})^n)$ is the Jacobian matrix with regard to the gradient of each component of deformed deformation fields $p(\boldsymbol{x})$ and $q(\boldsymbol{x})$.

### 3.2 Numerical solution on L1 sparsity-inducing norm

The L1 optimization problem has been used and exploited in several areas. One reason for this is its high computation intractability, and another reason is that it requires techniques that are very problem-specific. In our model, we adopt a fast iterative shrinkage thresholding framework which was presented by Beck and Teboulle (2008). It has a global rate of convergence that was significantly improved compared with the classical methods. By setting the gradient with regard to $b$ as 0, we obtain

$$\begin{aligned}\frac{\partial E}{\partial b(\boldsymbol{x})}&=\beta(p(\boldsymbol{x})+q(\boldsymbol{x}+p(\boldsymbol{x}))+b(\boldsymbol{x}))+\varepsilon\,\mathrm{sgn}(b(\boldsymbol{x}))\\&=0\\\Rightarrow b(\boldsymbol{x})&=-(p(\boldsymbol{x})+q(\boldsymbol{x}+p(\boldsymbol{x})))-\frac{\varepsilon}{\beta}\mathrm{sgn}(b(\boldsymbol{x}))\\&=\mathrm{shrink}\left(-(p(\boldsymbol{x})+q(\boldsymbol{x}+p(\boldsymbol{x}))),\frac{\varepsilon}{\beta}\right),\end{aligned}\tag{12}$$

where $\mathrm{sgn}(b(\boldsymbol{x}))$ indicates the sign of $b(\boldsymbol{x})$, which means $\mathrm{sgn}(b(\boldsymbol{x}))=1$ if $b(\boldsymbol{x})>0$ and $\mathrm{sgn}(b(\boldsymbol{x}))=-1$ otherwise. This shrink operator provides a strategy to yield an estimation of the components to reach non-zero in an optimal solution, and it is defined as

$$\begin{aligned}&\mathrm{shrink}(-(p(\boldsymbol{x})+q(\boldsymbol{x}+p(\boldsymbol{x}))))\\&=\mathrm{sgn}(-(p(\boldsymbol{x})+q(\boldsymbol{x}+p(\boldsymbol{x}))))\\&\quad\cdot\max\left(\left|-(p(\boldsymbol{x})+q(\boldsymbol{x}+p(\boldsymbol{x})))\right|-\frac{\varepsilon}{\beta},0\right).\end{aligned}$$

Fig. 1 is the main algorithm flow of the proposed algorithm.

## 4 Experimental results

### 4.1 Image matching accuracy and inverse consistency

In this subsection, we show the utility of our proposed model in quantifying the temporal evolution of image matching criteria. Our technique is applied to two normal 3D magnetic resonance (MR) brain

Initialize $p$, $q$, $b$, $c$
**for** $i$=1:$M$ **do**
  Forward image registration (source: $\boldsymbol{I}_0$; target: $\boldsymbol{I}_1$)
    Step 1: Update dual variable $u$ in forward registration by Eq. (8)
    Step 2: Update incremental variable $\Delta p$ by Eq. (11)
    Step 3: Compute sparsity term $b$ by Eq. (12)
  Backward image registration (source: $\boldsymbol{I}_1$; target: $\boldsymbol{I}_0$)
    Repeat steps 1–3 for updating $u$ in backward registration, $\Delta q$, and $c$
**end**

**Fig. 1 Main algorithm flow**

scans acquired from two persons, one aged 3 and the other aged 38. To obtain a smooth and accurate match for these sets of experimental data, we set smoothness parameters $\lambda$, $\gamma$ to 0.05, inverse consistent parameters $\beta$, $\eta$ to 0.01, and factors $\varepsilon$, $\theta$ to 0.001. Fig. 2 shows the original source and target images as well as the forward and backward deformed images.

The different scaling levels of brain shape and the large topological changes in the white matter usually cause problems in traditional image registration models. Our methodology resolves the problems caused by these topographical changes and decreases the consistent error of forward and backward transformations, which is demonstrated in Fig. 2. Experimental results show that our method is able to jointly estimate forward and backward transformations, which makes the forward and backward transformations invertible. An additional benefit of our model is that the topology of the transformation is preserved. In general, the transformation between the large deformation images should result in continuous differentiable one-to-one mapping, to preserve the topology. Non-negative determinate Jacobian fields in Fig. 2 show that our model produces diffeomorphic and topology preserving maps between images.

To demonstrate the ability of our method to find an optimal, smooth deformation, we applied it to a series of 73 frames of moving camera video and analyzed the real-time deformation and direction vectors of pixels over time. An example of video frames and related deformation fields is shown in Fig. 3. We set $\beta$, $\eta$ to 0.01 to enforce the invertible property on deformation fields, and $\varepsilon$, $\theta$ to 0.001 to control the sparsity. Another advantage that our model has over the traditional elastic model is that, discontinuities are preserved rather than over-smoothed; for example,

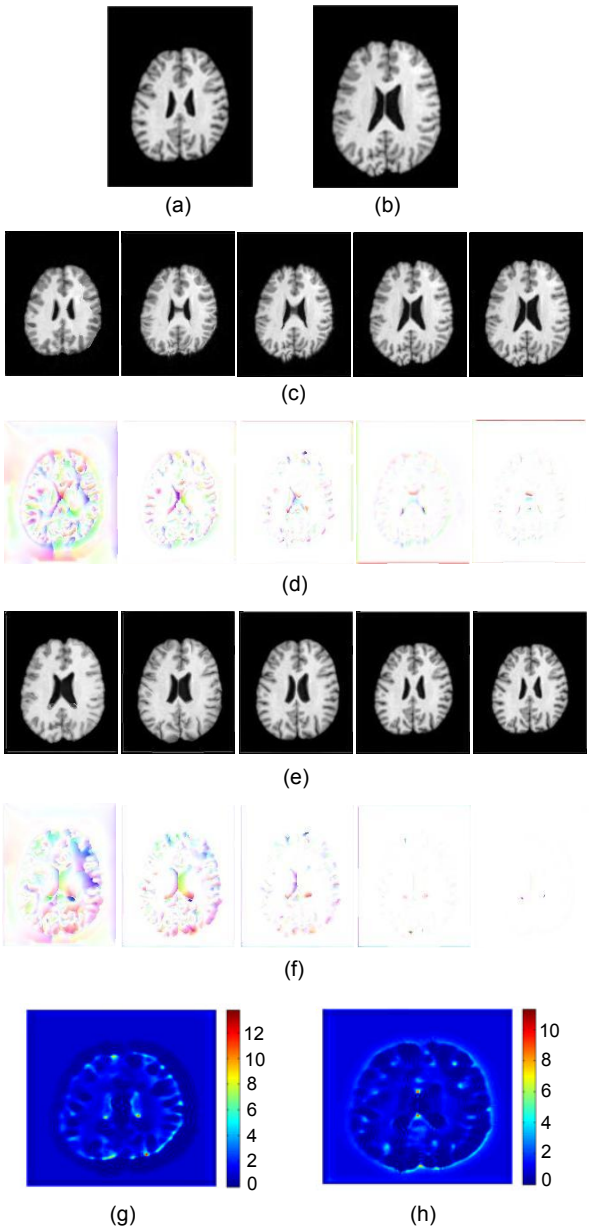


**Fig. 2 Demonstration of forward and backward transformations between two images**

(a) is the template image $\boldsymbol{I}_0$ and (b) is the target image $\boldsymbol{I}_1$. (c) is the time series of forward transformation from template to target images and (d) is the consistent error between each deformed template $\boldsymbol{I}_0$ and target $\boldsymbol{I}_1$ in forward transformation. (e) is the time series of backward transformation from target to template images and (f) is the consistent error between each deformed template $\boldsymbol{I}_1$ and target $\boldsymbol{I}_0$ in backward transformation. (g) is the determinant of the Jacobian fields for forward transformation and (h) for backward transformation

transformation on the edge of images is well constrained. A comparison of the deformation fields is also given in Fig. 3.


**Fig. 3 Comparison of deformation fields calculated using the proposed algorithm and the traditional algorithm without penalty terms**

(a) The 2nd, 6th, 10th, 19th, 27th frames of video series; (b) Corresponding deformation fields using the proposed algorithm; (c) Corresponding deformation fields using the traditional algorithm with no penalty term

## 4.2 Sparsity-inducing influence

In the following experiments, we first tested our proposed model on a set of synthetic data (size 50×50). Fig. 4 illustrates image change caused by global deformation and local infiltration. The smoothness parameters $\lambda$, $\gamma$ were set to 0.01, inverse consistent parameter $\beta$, $\eta$ 0.01, and factors $\varepsilon$, $\theta$ 0.005.

By using our method, image matching between the template and the target is processed appropriately by leaving the infiltration area. The sparsity-inducing term in our methodology controls the local deformation of geometric metamorphosis, which hinders global image registration. Conversely, from the grid information of deformation in Fig. 4, the infiltration part is well detected in our system, which is of great utility in clinical medical imaging, for instance, brain tumor tracking and TBI detection.

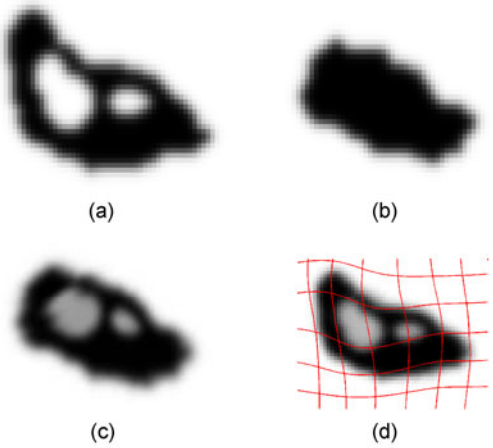


**Fig. 4 Results on synthetic data (the movement and the hole which leads to image appearance change are well detected)**

(a) Template image $\boldsymbol{I}_0$; (b) Target image $\boldsymbol{I}_1$; (c) Deformed template image; (d) Grid information for deformation field from $\boldsymbol{I}_0$ to $\boldsymbol{I}_1$

To demonstrate the application of the proposed method in solving practical problems, we used real TBI data (size 128×128×128). We considered the TBI data set of two images obtained from human subjects (Fig. 5). A rigid transformation was applied to remove rotations, translations, or reflections. In these pathological images, the large differences inside the brain (highlighted by a white circle) normally cause a large mis-registration (Fig. 6), despite the similarity in the procedure of acquiring these images. Results in Fig. 5 show that our method precisely detects both global deformation and local infiltration in 3D brain image registration. The deformation grid also presents fairly smooth forward and backward transformations. The parameters we used in this experiment were: $\lambda$=$\gamma$=0.05, $\beta$=$\eta$=0.06, and $\varepsilon$=$\theta$=0.01.

We showed the registration accuracy and processing time of our method on the TBI images. Comparisons were made with the traditional consistent image registration (Christensen and Johnson, 2001), large deformation diffeomorphic metric mapping (LDDMM) (Beg *et al*., 2005), and stationary velocity field (SVF) (Hernandez *et al.*, 2008) methods. Table 1 shows the comparison of registration accuracy as measured by the average of the mean squared errors (MSEs) between the forward and backward registrations. In addition, we show the convergence graph of each model in Fig. 7. It indicates that our

method converges to a smaller error with fewer iterations than LDDMM and SVF. However, the convergence fails in the traditional consistent image registration method. As shown in Fig. 7 (blue line), the jump occurs around iteration 80, and will appear later as the iteration goes on. Table 2 shows the processing time of each method.

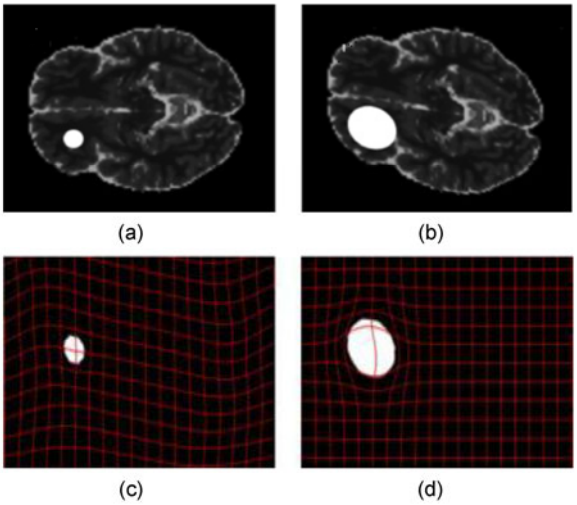


**Fig. 5 Results on TBI images with infiltration**
(a) and (b) are TBI images with different infiltration; (c) Deformation field of forward transformation; (d) Deformation field of backward transformation

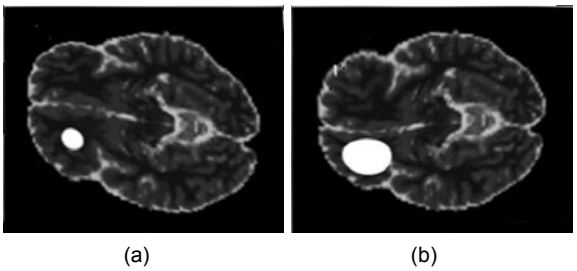


**Fig. 6 Classical image registration results (the template and target images are the same as those in Fig. 5)**
(a) Forward transformation; (b) Backward transformation

**Table 1 Comparison of the average registration MSEs obtained using four different methods**

| Method | Average registration MSE | |
|---|---|---|
| | Forward | Backward |
| Consistent image registration | 0.089 | 0.144 |
| LDDMM | 0.070 | 0.134 |
| SVF | 0.091 | 0.156 |
| Proposed | 0.040 | 0.048 |

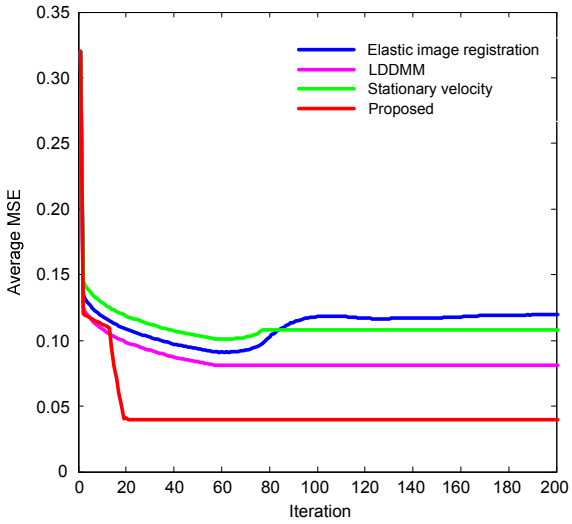


**Fig. 7 Convergence of forward registration using elastic image registration, LDDMM, stationary velocity, and the proposed algorithm**
References to color refer to the online version of this figure

**Table 2 Processing time of forward registration obtained using four different methods**

| Method | Processing time (s) |
|---|---|
| Consistent image registration | 4.8 |
| LDDMM | 960.0 |
| SVF | 7.0 |
| Proposed | 6.6 |

## 5 Conclusions

This paper presents a new algorithm for image registration with geometric changes. A sparsity-inducing penalty was proposed to regularize the geometric change (non-invertible) region in an effective global framework. A new energy optimization scheme derived from the inverse consistent principle was analyzed. It preserved topology and uniquely described the correspondences between two matching images. A numerical method was applied to speed up the convergence and enhance the stability of the algorithm. Experimental results on real TBI image data demonstrated that our proposed approach can effectively reduce the side effects of geometric change. The sparsity-inducing penalty made a significant contribution to global deformation computation. The ability to optimize and control metamorphosis in the

geometric approach could produce many interesting opportunities for new applications and analyses in the medical imaging area. In the future we aim to conduct further research in this area with the expectation of applying our approach in an atlas building framework.

## References


Bajcsy, R., Broit, C., 1982. Matching of deformed images. Proc. 6th Int. Conf. on Pattern Recognition, p.351-353.

Beck, A., Teboulle, M., 2008. A fast iterative shrinkage-thresholding algorithm for linear inverse problems. *SIAM J. Imag. Sci.*, **2**(1):183-202. [doi:10.1137/080716542]

Beg, M.F., Miller, M.I., Trouvé, A., *et al.*, 2005. Computing large deformation metric mappings via geodesic flows of diffeomorphisms. *Int. J. Comput. Vis.*, **61**(2):139-157. [doi:10.1023/B:VISI.0000043755.93987.aa]

Chambolle, A., 2004. An algorithm for total variation minimization and applications. *J. Math. Imag. Vis.*, **20**(1): 89-97. [doi:10.1023/B:JMIV.0000011325.36760.1e]

Christensen, G.E., Johnson, H.J., 2001. Consistent image registration. *IEEE Trans. Med. Imag.*, **20**(7):568-582. [doi:10.1109/42.932742]

Christensen, G.E., Rabbitt, R.D., Miller, M.I., 1996. Deformable templates using large deformation kinematics. *IEEE Trans. Image Process.*, **5**(10):1435-1447. [doi:10.1109/83.536892]

Hall, E.L., 1979. Computer Image Processing and Recognition. Academic Press, New York, USA.

Herbin, M., Venot, A., Devaux, J.Y., *et al.*, 1989. Automated registration of dissimilar images: application to medical imagery. *Comput. Vis. Graph. Image Process.*, **47**(1): 77-88. [doi:10.1016/0734-189X(89)90055-8]

Hernandez, M., Olmos, S., Pennec, X., 2008. Comparing algorithms for diffeomorphic registration: stationary LDDMM and diffeomorphic demons. Proc. 2nd MICCAI Workshop on Mathematical Foundations of Computational Anatomy, p.24-35.

Lucas, B.D., Kanade, T., 1981. An iterative image registration technique with an application to stereo vision. Proc. 7th Int. Joint Conf. on Artificial Intelligence, p.121-130.

Luck, J., Little, C., Hoff, W., 2000. Registration of range data using a hybrid simulated annealing and iterative closest point algorithm. Proc. IEEE Int. Conf. on Robotics and Automation, p.3739-3744. [doi:10.1109/ROBOT.2000.845314]

Niethammer, M., Hart, G.L., Pace, D.F., *et al.*, 2011. Geometric metamorphosis. Proc. 14th Int. Conf. on Medical Image Computing and Computer-Assisted Intervention, p.639-646. [doi:10.1007/978-3-642-23629-7_78]

Richard, F.J.P., Samson, A.M.M., 2007. Metropolis-Hasting techniques for finite-element-based registration. Proc. IEEE Conf. on Computer Vision and Pattern Recognition, p.1-6. [doi:10.1109/CVPR.2007.383422]

Rudin, L.I., Osher, S., Fatemi, E., 1992. Nonlinear total variation based noise removal algorithms. *Phys. D*, **60**(1-4): 259-268. [doi:10.1016/0167-2789(92)90242-F]

Trouvé, A., Younes, L., 2005. Metamorphoses through Lie group action. *Found. Comput. Math.*, **5**(2):173-198. [doi:10.1007/s10208-004-0128-z]

Zhang, M., Singh, N., Fletcher, P.T., 2013. Bayesian estimation of regularization and atlas building in diffeomorphic image registration. Proc. 23rd Int. Conf. on Information Processing in Medical Imaging. p.37-48. [doi:10.1007/978-3-642-38868-2_4]